Nanoscale

RSC Publishing

PAPER

View Article Online
View Journal | View Issue

Cite this: *Nanoscale*, 2013, **5**, 2107

Multifunctional Fe_3O_4–TiO_2 nanocomposites for magnetic resonance imaging and potential photodynamic therapy

Leyong Zeng,[a] Wenzhi Ren,[a] Lingchao Xiang,[a] Jianjun Zheng,[b] Bin Chen[b] and Aiguo Wu*[a]

Received 7th December 2012
Accepted 4th January 2013

DOI: 10.1039/c3nr33978e

www.rsc.org/nanoscale

Multifunctional Fe_3O_4–TiO_2 nanocomposites with Janus structure for magnetic resonance imaging (MRI) and potential photodynamic therapy (PDT) were synthesized, in which Fe_3O_4 was used as a MRI contrast agent and TiO_2 as an inorganic photosensitizer for PDT. Their morphology, structure, and MRI and PDT performance were characterized, respectively. Moreover, the location of Fe_3O_4–TiO_2 nanocomposites in MCF-7 cells was also investigated by the staining of Prussian blue and alizarin red, respectively. The results showed that the as-prepared Fe_3O_4–TiO_2 nanocomposites had good T_2-weighted MRI performance, and the MCF-7 cells incubated with nanocomposites could be killed under the irradiation of UV light. Compared with traditional organic photosensitizers, TiO_2 inorganic photosensitizers could have more stable PDT performance due to their nanoscale size and anti-photodegradable stability. Therefore, the as-prepared Fe_3O_4–TiO_2 nanocomposites could have potential applications as a new kind of multifunctional agent for both MRI and PDT.

Introduction

Magnetic resonance imaging (MRI), computed tomography (CT) imaging and ultrasound (US) imaging are the most important imaging techniques in clinical medicine. It is well known that MRI is a noninvasive imaging technique and fit for the tumor diagnosis of internal organs, for example, liver, lung, breast, *etc.* With the use of MRI contrast agents, some tumors could be early diagnosed. During the past two decades, superparamagnetic iron oxides have attracted a great deal of attention due to their important application as MRI contrast agents.[1–7] Recently, molecular imaging, diagnostics and therapy based on nanomaterials have become a promising field, which would have potential applications in clinical diagnostics and therapy for cancer.[8–10] In particular, MRI contrast agents have been developed towards multimodal imaging and multifunction for imaging and therapy. For example, Gd@Fe_3O_4, PLA@-Fe_3O_4 and Fe_3O_4@Au have been investigated as T_1- and T_2-weighted MRI, MRI-US and MRI-CT dual-mode imaging contrast agents, respectively.[11–14] Moreover, Fe_3O_4@Au could also be used as MRI contrast agents and photothermal therapy agents.[15–17] Furthermore, when MRI contrast agents were coupled with photosensitizers, they could be used as photodynamic therapy (PDT) agents under light excitation with some specific wavelength.[18–20] Therefore, in order to realize the real-time imaging and *in situ* therapy for cancer, it was very interesting to develop a multifunctional agent of MRI and PDT.

Generally, most of the photosensitizers are organic macromolecules or complexes used in PDT.[21–23] However, they could have a short maintenance time in the body, and they might be decomposed under no light irradiation. It is well known that TiO_2 nanoparticles are a kind of typical inorganic photosensitizer, which have been widely used as a photocatalyst in environmental sciences. Under the excitation of UV light, the light-induced electrons and holes of TiO_2 nanocrystals with anatase structure will be divided, and then the contamination could be degraded. Furthermore, TiO_2 nanoparticles could also be used as a PDT agent in biomedical fields. Under the irradiation of UV light, the free radicals and singlet oxygen produced by TiO_2 nanoparticles could produce light toxicity and then destroy the tissues and cancer cells.[24,25] Moreover, TiO_2 nanoparticles could be maintained for a longer time in the body than that of traditional organic photosensitizers, and they were nontoxic and stable under no light irradiation. Few investigations have also been reported about the application of TiO_2 nanoparticles as inorganic photosensitizers for PDT.[25–32]

Therefore, the MRI performance of Fe_3O_4 and the inorganic PDT performance of TiO_2 nanoparticles were very useful for the development of a multifunctional agent of MRI and PDT. In the process of diagnosis and therapy, UV light was brought into the location of cancer cells using an UV fiber. Then using an

[a]*Key Laboratory of Magnetic Materials and Devices, Division of Functional Materials and Nanodevices, Ningbo Institute of Materials Technology and Engineering, Chinese Academy of Sciences, Ningbo 315201, China. E-mail: aiguo@nimte.ac.cn; Fax: +86 574 86685163; Tel: +86 574 86685039*

[b]*Ningbo No. 2 Hospital, Ningbo 315000, China*

on-operation MRI technique, the real-time MRI and *in situ* PDT could be realized. Therefore, the Fe_3O_4–TiO_2 nanocomposites would have important applications in the MRI and PDT of cancer in future.

In this paper, multifunctional Fe_3O_4–TiO_2 nanocomposites were synthesized, which could be used as a multifunctional agent of MRI and inorganic photosensitizers for PDT. The morphology, microstructure, and magnetic property of Fe_3O_4–TiO_2 nanocomposites were characterized by transmission electron microscopy (TEM), high-resolution transmission electron microscopy (HRTEM) with energy dispersed X-ray spectroscopy (EDS), X-Ray Diffraction (XRD) and the physical performance measurement system (PPMS). Moreover, the MRI and PDT performances were investigated by MR imaging, relaxivity and the methylthiazol tetrazolium (MTT) assay method. Furthermore, using the staining of Prussian blue and alizarin red, respectively, the location of Fe_3O_4–TiO_2 nanocomposites in MCF-7 cells was also observed by using a biomicroscope and a laser scanning confocal microscope.

Experimental

a Preparation of Fe_3O_4–TiO_2 nanocomposites

In this experiment, ferric acetylacetonate ($Fe(acac)_3$) and tetrabutyl titanate (TBOT) were used as reaction agents, and oleic acid (OA), oleylamine (OM), *n*-octyl alcohol and ethanol were used as solvents and dressing agents. All agents were purchased from Aladdin Ltd.

Fe_3O_4–TiO_2 nanocomposites were synthesized by the solvent-thermal method. First, TiO_2 nanoparticles with about 5–10 nm were synthesized based on the previously reported method.[33] Then the as-prepared TiO_2 nanoparticles were centrifuged and washed with ethanol three times, and were re-dispersed in *n*-hexane. Next, 0.5 mmol of $Fe(acac)_3$ were dissolved in 4 mL of OM and 12 mL of *n*-octyl alcohol, and 1 mmol of TiO_2 nanoparticles dispersed in *n*-hexane were dropped into the above $Fe(acac)_3$ solution. The mixtures were being stirred for 4 h, and then the temperature was increased to 70 °C in order to evaporate the *n*-hexane. Finally, they were cooled to room temperature, and were transferred into a reaction kettle. The reaction temperature was kept at 240 °C, and the time was 2 h. Finally, the as-prepared Fe_3O_4–TiO_2 nanocomposites were centrifuged, washed with ethanol 3 times, and were dispersed into the water phase by PEG coating.

b UV irradiation

First, MCF-7 cells were seeded in a 96-well plate, and then incubated with Fe_3O_4–TiO_2 nanocomposites. Finally, the MTT assay method was used to investigate the cell viability pre- and post-UV irradiation at different times. The power density of UV light was 25 mW cm^{-2}, and the distance between the UV light and cells was 20 cm. The concentrations of Fe_3O_4–TiO_2 nanocomposites were 50, 100, 150 and 200 μg mL^{-1}, respectively, and the incubation time of Fe_3O_4–TiO_2 nanocomposites in MCF-7 cells was about 24 h. When they were incubated for 6 h, UV irradiation was carried out, and the irradiation time was 5 min, 10 min, and 15 min, respectively. Furthermore, as control, MCF-7 cells without Fe_3O_4–TiO_2 nanocomposites were also irradiated by UV light with the time of 5 min, 10 min, and 15 min, respectively.

c Staining of cells

Prussian blue and alizarin red dyes were used respectively for the staining of MCF-7 cells. The first part is Prussian blue staining of MCF-7 cells incubated with Fe_3O_4–TiO_2 nanocomposites. The concentration of nanocomposites was 100 μg mL^{-1}, and the incubation time was 24 h. The procedure for Prussian blue staining was followed according to previous articles.[34,35] The second part is alizarin red staining. The Fe_3O_4–TiO_2 nanocomposites were stirred with alizarin red solution for 8 h, and then they were centrifuged and washed with water three times. Finally, they were re-dispersed in PBS buffers. The concentration of nanocomposites was 100 μg mL^{-1}, and the incubation time was 4 h.

d Characterization

The morphology, microstructure and magnetic property of the as-prepared Fe_3O_4–TiO_2 nanocomposites were characterized by using a Tecnai F20 transmission electron microscope (TEM) with EDS accessory, a Bruker AXS D8 X-Ray Diffractometer and Quantum Design Model-9 PPMS. The MR imaging and relaxivity performance of Fe_3O_4–TiO_2 nanocomposites were tested by using a Siemens Avanto MRI scanner system with a magnetic field of 1.5 T and a Mico MR Analyzing system (Shanghai Niumag Corporation) with a magnetic field of 0.47 T, respectively. Finally, based on MCF-7 cells, the cell viability of the as-prepared Fe_3O_4–TiO_2 nanocomposites pre- and post-UV irradiation was characterized by the MTT assay method, and the location of nanocomposites in MCF-7 cells was also investigated using the staining of Prussian blue and alizarin red dyes by using a biomicroscope and a Leica laser scanning confocal microscope, respectively.

Results and discussion

Fig. 1 shows the TEM, HRTEM and EDS images of the as-prepared Fe_3O_4–TiO_2 nanocomposites. As shown in Fig. 1(a), the dispersity of Fe_3O_4–TiO_2 nanocomposites was good, and the Fe_3O_4–TiO_2 nanocomposites did not have a core–shell structure. Closer observation of Fig. 1(b) reveals that most of the Fe_3O_4–TiO_2 nanocomposites had a Janus structure, and the single size of the Fe_3O_4–TiO_2 nanocomposites was about 30–40 nm. In Fig. 1(c), the HRTEM image of Fe_3O_4–TiO_2 nanocomposites shows that Fe_3O_4 was coupled with TiO_2 nanoparticles to form a Janus structure. Moreover, the interplanar distance of two parts was 0.2518 nm and 0.3517 nm, respectively, which corresponded well with the (311) plane of Fe_3O_4 and the (101) plane of TiO_2, respectively. Fig. 1(d) shows the EDS spectrum of the Fe_3O_4–TiO_2 nanocomposite. The peaks of C, Cu, O, Fe, and Ti elements could be found, in which the elements of C and Cu were from a copper grid with carbon

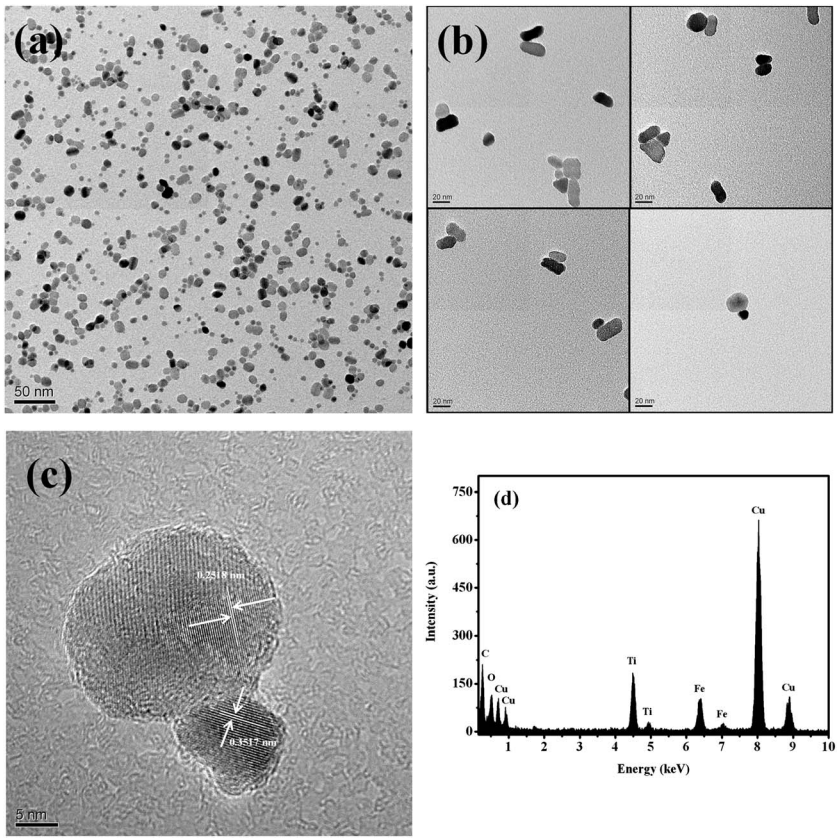

Fig. 1 TEM, HRTEM and EDS images of Fe_3O_4–TiO_2 nanocomposites. (a and b) TEM; (c) HRTEM; (d) EDS.

films, and the elements of Fe, O and Ti were from the Fe_3O_4–TiO_2 nanocomposite.

The crystal structure and magnetic property of the as-prepared Fe_3O_4–TiO_2 nanocomposites were also characterized. Fig. 2(a) shows the XRD spectra of Fe_3O_4, TiO_2 and Fe_3O_4–TiO_2 nanocomposites. It could be observed that the peaks of Fe_3O_4–TiO_2 nanocomposites included the peaks of Fe_3O_4 with cubic structure and the peaks of TiO_2 with anatase structure. Fig. 2(b) shows the M–H curves of Fe_3O_4 and Fe_3O_4–TiO_2 nanocomposites. The results showed that the as-prepared Fe_3O_4 and Fe_3O_4–TiO_2 nanocomposites had superparamagnetism, and the saturation magnetization of Fe_3O_4 and Fe_3O_4–TiO_2 nanocomposites was 58.95 and 14.90 emu g^{-1}, respectively.

The MRI performance of the as-prepared Fe_3O_4–TiO_2 nanocomposites was characterized by using a Siemens Avanto MRI scanning system with a magnetic field of 1.5 T. Fig. 3 shows the T_1- and T_2-weighted MR images of Fe_3O_4–TiO_2 nanocomposites. From left to right, the Fe concentrations were 0, 0.2, 0.4, 0.8, 1.2, 1.6 and 2 mM, respectively. As shown in Fig. 3(b), the T_2-weighted MR images of Fe_3O_4–TiO_2 nanocomposites were darker, compared with the MR image of water. Moreover, by increasing the concentration of Fe_3O_4–TiO_2 nanocomposites, the MR images got darker and darker. However, in Fig. 3(a), the T_1-weighted MR images were not changed obviously, compared with that of water. Therefore, the results indicated that the as-prepared Fe_3O_4–TiO_2 nanocomposites have good T_2-weighted MRI performance.

In order to further quantitatively analyze the MRI performance, the MR relaxation properties of Fe_3O_4–TiO_2 nanocomposites were investigated by using a MR analyzing system with a magnetic field of 0.47 T (Shanghai Niumag Micro MR). By MR relaxivity measurement of Fe_3O_4–TiO_2 nanocomposites with different concentrations, the longitudinal and transverse relaxivities (*i.e.* r_1 and r_2 values) of Fe_3O_4–TiO_2 nanocomposites could be calculated. Fig. 4(a) and (b) show the plots of $1/T_1$ and $1/T_2$ *versus* concentrations of the as-prepared Fe_3O_4–TiO_2 nanocomposites. By calculation, the r_1 and r_2 values of Fe_3O_4–TiO_2 nanocomposites were 1.444 and 54.691 mM^{-1} s^{-1}, respectively. Because the ratio of r_2/r_1 values was more than 3, the as-prepared Fe_3O_4–TiO_2 nanocomposites had good T_2-weighted MR performance, which also corresponded to that of MR images.

Using the staining method of cells, the location of nanocomposites in cells could be observed and analyzed. In this work, MCF-7 cells were incubated with Fe_3O_4–TiO_2 nanocomposites, which were stained by Prussian blue and alizarin red, respectively. The concentration of Fe_3O_4–TiO_2 nanocomposites was 100 μg mL^{-1}, and the incubation time in MCF-7 cells was 24 h and 4 h for the staining of Prussian blue and alizarin red, respectively. Fig. 5 shows the photomicrographs of MCF-7 cells stained by Prussian blue without and with the incubation of Fe_3O_4–TiO_2 nanocomposites. As shown in Fig. 5(a), the MCF-7 cells stained by Prussian blue were not blue when they were not incubated with Fe_3O_4–TiO_2

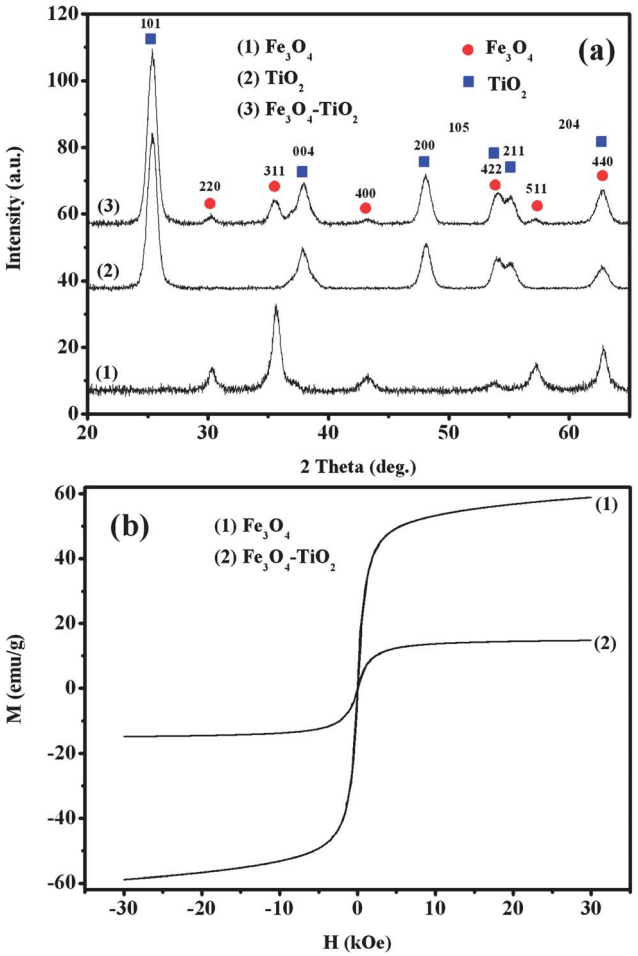

Fig. 2 XRD spectra and M–H curves of Fe_3O_4–TiO_2 nanocomposites. (a) XRD spectra; (b) M–H curves.

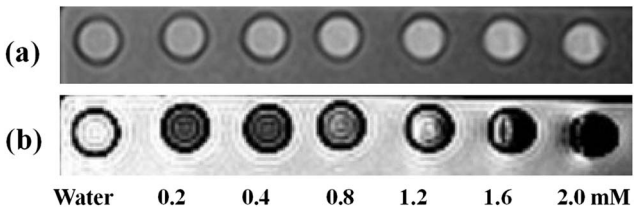

Fig. 3 T_1- and T_2-weighted MR images of Fe_3O_4–TiO_2 nanocomposites. (a) T_1-weighted MR images; (b) T_2-weighted MR images. Imaging parameters for the FLASH sequence were TR = 600 ms, TE = 7 ms for T_1 and TR = 3000 ms, TE = 90 ms for T_2, respectively.

nanocomposites. However, as shown in Fig. 5(b), with the incubation of Fe_3O_4–TiO_2 nanocomposites, the colour of MCF-7 cells stained by Prussian blue was blue, which indicated that most of the Fe_3O_4–TiO_2 nanocomposites had entered into MCF-7 cells. In Fig. 5(c), some Fe_3O_4–TiO_2 nanocomposites and their clusters could be observed obviously in the cytoplasm of the labeled cells.

Fig. 6 shows the confocal microscopy images of MCF-7 cells stained by alizarin red without and with the incubation of Fe_3O_4–TiO_2 nanocomposites. Fig. 6(a)–(c) show the images of

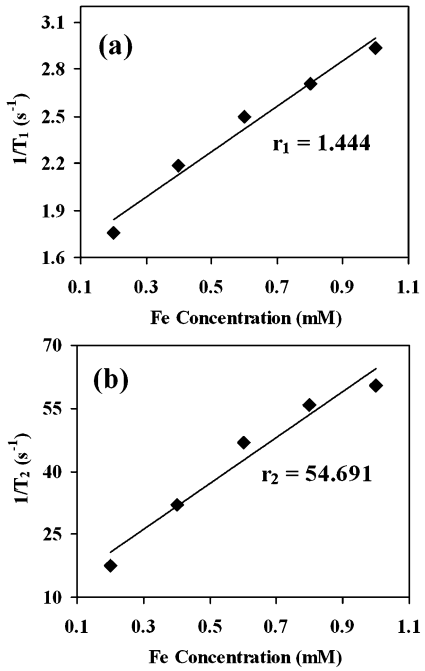

Fig. 4 Longitudinal (a) and transverse (b) relaxivities of Fe_3O_4–TiO_2 nanocomposites.

the cell nucleus, alizarin red, and the overlap of the cell nucleus and alizarin red, respectively. In Fig. 6(b) and (c), a red image could not be observed around the cell nucleus, which indicated that the alizarin red dyes could not be stained on the cells when they were not coupled with Fe_3O_4–TiO_2 nanocomposites. However, when MCF-7 cells were incubated with Fe_3O_4–TiO_2 nanocomposites coupled with alizarin red dyes, Fe_3O_4–TiO_2 nanocomposites could be located in the cytoplasm of the labeled cells, as shown in Fig. 6(e) and (f). The results of staining of cells by Prussian blue and alizarin red dyes showed that the as-prepared Fe_3O_4–TiO_2 nanocomposites could be located easily in the MCF-7 cells, which indicated that they had good biocompatibility.

Furthermore, under the irradiation of UV light with different time, the cell viability of MCF-7 cells incubated with Fe_3O_4–TiO_2 nanocomposites was also investigated using MTT assay method. The incubation time of Fe_3O_4–TiO_2 nanocomposites in MCF-7 cells was 24 h, and the concentrations of Fe_3O_4–TiO_2 nanocomposites were 50, 100, 150, and 200 μg mL^{-1}, respectively. As shown in Fig. 7(a), before they were irradiated by UV light, the cell viability was more than 90%, when the concentration of Fe_3O_4–TiO_2 nanocomposites was less than 100 μg mL^{-1}, and the cell viability was still more than 85% when the concentration was between 100 and 200 μg mL^{-1}. The results showed that the as-prepared Fe_3O_4–TiO_2 nanocomposites had low cytotoxicity when the incubation time of nanocomposites was 24 h. However, when they were irradiated under UV light for 5 min, 10 min, and 15 min, respectively, it could be observed that the cell viability had decreased obviously with the increase of irradiation time. Moreover, under the irradiation of UV light, the concentration of Fe_3O_4–TiO_2 nanocomposites had an important influence on the cell viability of MCF-7 cells. When the

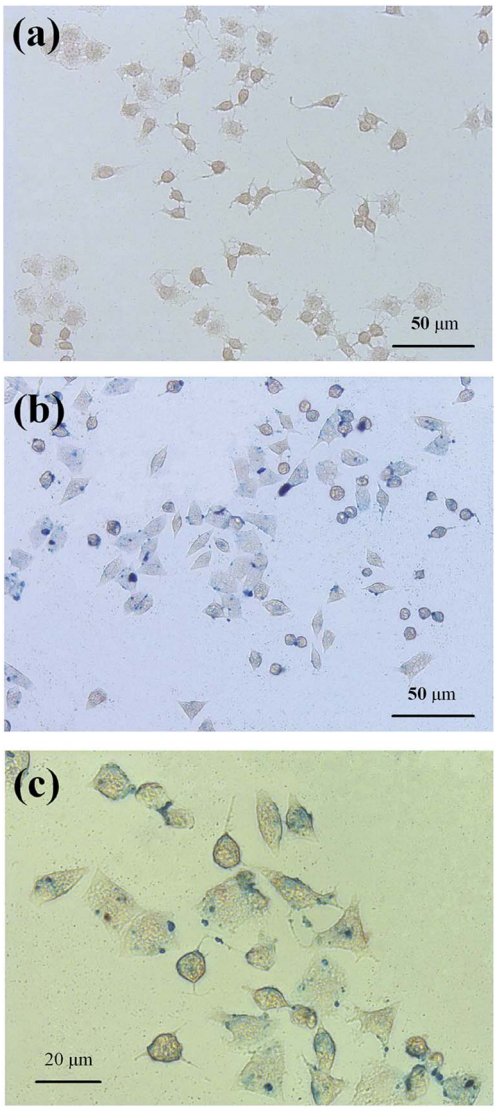

Fig. 5 Photomicrographs of MCF-7 cells stained by Prussian blue. (a) Control; (b and c) MCF-7 cells incubated with Fe_3O_4–TiO_2 nanocomposites.

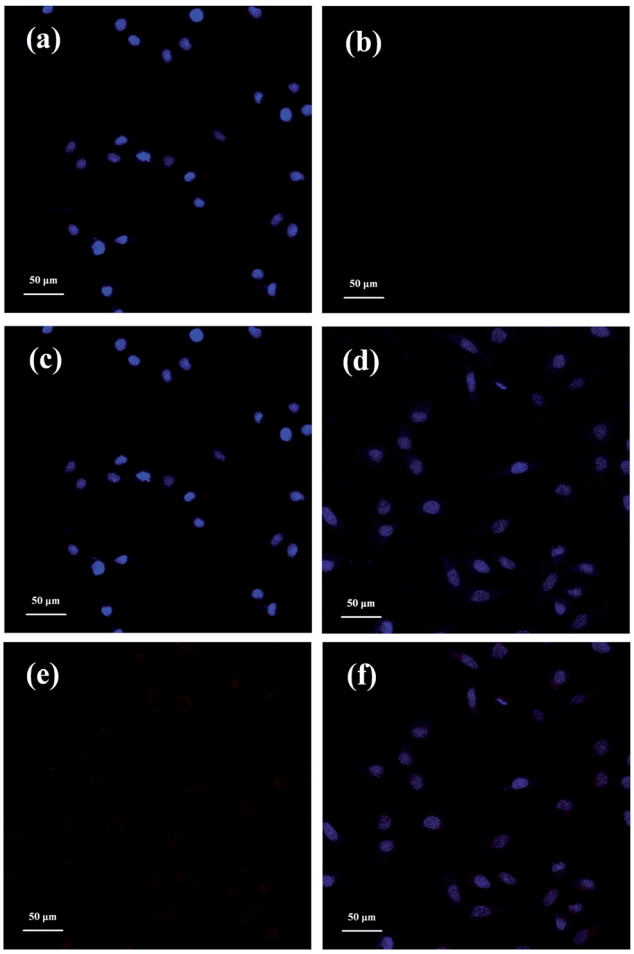

Fig. 6 Confocal microscopy images of MCF-7 cells stained by alizarin red. (a–c) Control; (d–f) MCF-7 cells incubated with Fe_3O_4–TiO_2 nanocomposites.

concentration of Fe_3O_4–TiO_2 nanocomposites was less than 100 μg mL^{-1}, the cell viability was not obviously decreased, both pre- and post-irradiation. However, when the concentration was more than 100 μg mL^{-1}, the MCF-7 cells could be killed obviously under the irradiation of UV light. In Fig. 7, when the concentration of Fe_3O_4–TiO_2 nanocomposites was 200 μg mL^{-1}, it could be observed that the cell viability of pre-irradiation was about 85%, but was only about 55%, 49%, and 39% at the irradiation time of 5 min, 10 min and 15 min, respectively. Furthermore, the influence of UV light irradiation on the cell viability of MCF-7 cells was also investigated, when they were not incubated with Fe_3O_4–TiO_2 nanocomposites. Fig. 7(b) shows the cell viability of control MCF-7 cells, when the irradiation time of UV light was 0 min, 5 min, 10 min and 15 min, respectively. It could be observed that the cell viability was still more than 90%, compared with that of control MCF-7 cells without UV irradiation. The results indicated that Fe_3O_4–TiO_2 nanocomposites were critical for determination of cell viability under UV light irradiation. Moreover, the suitable concentration of Fe_3O_4–TiO_2 nanocomposites and the irradiation time of UV irradiation were very important for the PDT performance. Therefore, the Fe_3O_4–TiO_2 nanocomposites could be good inorganic photosensitizers for PDT in therapy for cancer in the future.

Based on the above results, the as-prepared Fe_3O_4–TiO_2 nanocomposites with Janus structure could be good MRI and PDT agents. The Janus structure could be important for the performance improvement of Fe_3O_4–TiO_2 nanocomposites. On one hand, the Janus structure could maintain the magnetism of Fe_3O_4–TiO_2 nanocomposites because the Fe_3O_4 magnetic part was not coated by TiO_2 nanoparticles, which could improve the MRI performance of Fe_3O_4–TiO_2 nanocomposites. On the other hand, under the irradiation of UV light, the light-induced electrons and holes of Fe_3O_4–TiO_2 nanocomposites with core–shell structure could be easily recombined, which would decrease the yield of free radicals and singlet oxygen.[36] However, due to the small interface between Fe_3O_4 and TiO_2 nanoparticles in Janus structure, the recombination of light-induced electrons and holes would be decreased, which could enhance the PDT efficiency. Furthermore, compared with traditional photosensitizers based on organic macromolecules or complexes, TiO_2-based inorganic photosensitizers had a longer

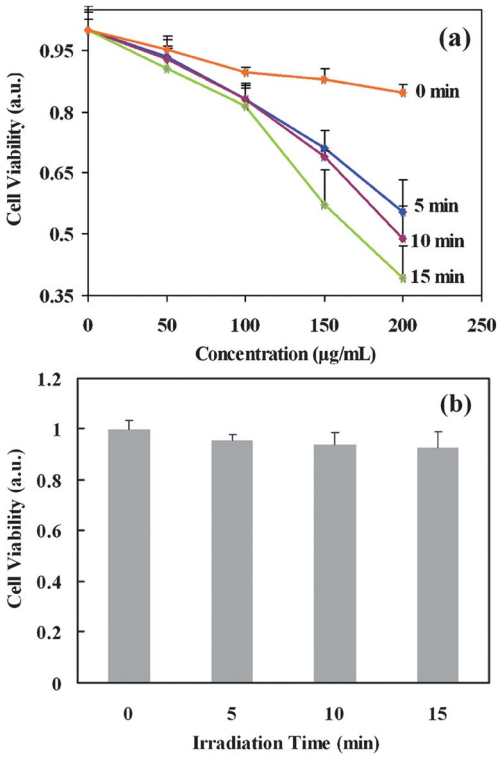

Fig. 7 Cell viability before and after UV light irradiation. (a) MCF-7 cells incubated with Fe_3O_4–TiO_2 nanocomposites; (b) MCF-7 cells without Fe_3O_4–TiO_2 nanocomposites.

maintenance time in the body and a more stable performance based on their nanoscale size. Therefore, the as-prepared Fe_3O_4–TiO_2 nanocomposites would be an excellent multifunctional agent of MRI and PDT and could have potential applications in the diagnosis and therapy of cancer in the future.

Conclusions

Using the MRI performance of Fe_3O_4 nanoparticles and the PDT performance of TiO_2 inorganic photosensitizers under the excitation of UV light, Fe_3O_4–TiO_2 nanocomposites could be used as a multifunctional agent of MRI and PDT. In this paper, Fe_3O_4–TiO_2 nanocomposites with Janus structure were synthesized. The size of the Janus Fe_3O_4–TiO_2 nanocomposites was about 30–40 nm, and the r_2 value was about 54.691 mM^{-1} s^{-1}. Moreover, under the irradiation of UV light, the cell viability incubated with Fe_3O_4–TiO_2 nanocomposites could be decreased from about 85% to 39%, compared with that without UV irradiation. Furthermore, the as-prepared Fe_3O_4–TiO_2 nanocomposites could be located easily in MCF-7 cells. Therefore, the Janus Fe_3O_4–TiO_2 nanocomposites could have potential applications as a multifunctional agent of MRI and PDT for the diagnosis and therapy of cancer in the future.

Acknowledgements

This work was supported by Natural Science Foundation of China (Grants no. 51102251 and 31170964), the aided program for Science and Technology Innovative Research Team of Ningbo Municipality (Grant no. 2009B21005), Ningbo Natural Science Foundation of China (Grant no. 2012A610113), Director Foundation of Ningbo Institute of Materials Technology and Engineering, and Hundred Talents Program of Chinese Academy of Sciences.

References

1 A. Figuerola, R. Corato, L. Manna and T. Pellegrino, *Pharmacol. Res.*, 2010, **62**, 126–143.
2 G. P. Yan, L. Robinson and P. Hogg, *Radiography*, 2007, **13**, e5–e19.
3 F. Q. Hu, L. Wei, Z. Zhou, Y. L. Ran, Z. Li and M. Y. Gao, *Adv. Mater.*, 2006, **18**, 2553–2556.
4 J. Lu, S. L. Ma, J. Y. Sun, C. C. Xia, C. Liu, Z. Y. Wang, X. N. Zhao, F. B. Gao, Q. Y. Gong, B. Song, X. T. Shuai, H. Ai and Z. W. Gu, *Biomaterials*, 2009, **30**, 2919–2928.
5 C. Yang, J. J. Wu and Y. L. Hou, *Chem. Commun.*, 2011, **47**, 5130–5141.
6 L. Y. Zeng, W. Z. Ren, J. J. Zheng, P. Cui and A. G. Wu, *Phys. Chem. Chem. Phys.*, 2012, **14**, 2631–2636.
7 N. Lee, Y. Choi, Y. Lee, M. Park, W. K. Moon, S. H. Choi and T. Hyeon, *Nano Lett.*, 2012, **12**, 3127–3131.
8 J. McCarthy, F. Jaffer and R. Weissleder, *Small*, 2006, **8–9**, 983–987.
9 C. Tassa, S. Y. Shaw and R. Weissleder, *Acc. Chem. Res.*, 2011, **44**, 842–852.
10 K. Y. Choi, G. Liu, S. Lee and X. Chen, *Nanoscale*, 2012, **21**, 330–342.
11 J. S. Choi, J. H. Lee, T. H. Shin, H. T. Song, E. Y. Kim and J. Cheon, *J. Am. Chem. Soc.*, 2010, **132**, 11015–11017.
12 H. Yang, Y. Zhuang, Y. Sun, A. Dai, X. Shi, D. Wu, F. Li, H. Hu and S. Yang, *Biomaterials*, 2011, **32**, 4584–4593.
13 F. Yang, Y. X. Li, Z. P. Chen, Y. Zhang, J. R. Wu and N. Gu, *Biomaterials*, 2009, **30**, 3882–3890.
14 E. Cheung, R. Alvares, W. Oakden, R. Chaudhary, M. Hill, J. Pichaandi, G. Mo, C. Yip, P. Macdonald, G. Stanisz, F. Veggel and R. Prosser, *Chem. Mater.*, 2010, **22**, 4728–4739.
15 W. J. Dong, Y. S. Li, D. C. Niu, Z. Ma, J. L. Gu, Y. Chen, W. R. Zhao, X. H. Liu, C. S. Liu and J. L. Shi, *Adv. Mater.*, 2011, **23**, 5392–5397.
16 R. Bardhan, W. Chen, C. Perez-Torres, M. Bartels, R. M. Huschka, L. L. Zhao, E. Morosan, R. G. Pautler, A. Joshi and J. Halas, *Adv. Funct. Mater.*, 2009, **19**, 3901–3909.
17 L. Cheng, K. Yang, Y. G. Li, X. Zeng, M. W. Shao, S. T. Lee and Z. Liu, *Biomaterials*, 2012, **33**, 2215–2222.
18 P. Huang, Z. M. Li, J. Lin, D. P. Yang, G. Gao, C. Xu, L. Bao, C. L. Zhang, K. Wang, H. Song, H. Y. Hu and D. X. Cui, *Biomaterials*, 2011, **32**, 3447–3458.
19 X. F. Qiao, J. C. Zhou, J. W. Xiao, Y. F. Wang, L. D. Sun and C. H. Yan, *Nanoscale*, 2012, **4**, 4611–4623.
20 J. Ding, J. H. Zhao, K. L. Cheng, G. F. Liu and D. H. Xiu, *J. Biomed. Nanotechnol.*, 2010, **6**, 683–686.
21 J. Shan, S. J. Budijono, G. Hu, N. Yao, Y. Kang, Y. Ju and R. K. Prud'homme, *Adv. Funct. Mater.*, 2011, **21**, 2488–2495.
22 P. Zhang, W. Steelant, M. Kumar and M. Scholfield, *J. Am. Chem. Soc.*, 2007, **129**, 4526–4527.

23 H. C. Guo, H. S. Qian, N. M. Idris and Y. Zhang, *Nanomedicine*, 2010, **6**, 486–495.
24 Q. Li, X. Wang, X. Lu, H. Tian, H. Jiang, G. Lv, D. Guo, C. Wu and B. Chen, *Biomaterials*, 2009, **30**, 4708–4715.
25 S. Yamaguchi, H. Kobayashi, T. Narita, K. Kanehira, S. Sonezaki, Y. Kubota, S. Terasaka and Y. Iwasaki, *Photochem. Photobiol.*, 2010, **86**, 964–971.
26 T. Paunesku, T. Rajh, G. Wiederrecht, J. Maser, S. Vogt, N. Stojicevic, M. Protic, B. Lai, J. Oryhon, M. Thurnauer and G. Woloschak, *Nat. Mater.*, 2003, **2**, 343–346.
27 K. Thurn, E. Brown, A. Wu, S. Vogt, B. Lai, J. Maser, T. Paunesku and G. Woloschak, *Nanoscale Res. Lett.*, 2007, **2**, 430–441.
28 E. Brown, T. Paunesku, A. Wu, K. Thurn, B. Haley, J. Clark, T. Priester and G. Woloschak, *Anal. Biochem.*, 2008, **383**, 226–235.
29 E. A. Rozhkova, I. Ulasov, B. Lai, N. M. Dimitrijevic, M. S. Lesniak and T. Rajh, *Nano Lett.*, 2009, **9**, 3337–3342.
30 J. W. Seo, H. Chung, M. Y. Kim, J. Lee, I. H. Choi and J. Cheon, *Small*, 2007, **3**, 850–853.
31 Q. Li, X. Wang, X. Lu, H. Tian, H. Jiang, G. Lv, D. Guo, C. Wu and B. Chen, *Biomaterials*, 2009, **30**, 4708–4715.
32 E. Stefanou, A. Evangelou and P. Falaras, *Catal. Today*, 2010, **151**, 58–63.
33 C. T. Dinh, T. D. Nguyen, F. Kleitz and T. O. Do, *ACS Nano*, 2009, **3**, 3737–3743.
34 W. Chen, P. Yi, Y. Zhang, L. Zhang, Z. Deng and Z. Zhang, *ACS Appl. Mater. Interfaces*, 2011, **3**, 4085–4091.
35 L. Y. Zeng, W. Z. Ren, J. J. Zheng, A. G. Wu and P. Cui, *Appl. Surf. Sci.*, 2012, **258**, 2570–2575.
36 B. Donia, A. Rose, K. Gary and M. Stephen, *J. Phys. Chem. B*, 2000, **104**, 4387–4396.